Available online at www.sciencedirect.com

ScienceDirect

Ceramics International 40 (2014) 1885–1891

CERAMICS INTERNATIONAL

www.elsevier.com/locate/ceramint

Effects of different organic additives on the formation of $YPO_4:Eu^{3+}$ nano-/microstructures under hydrothermal conditions with enhanced photoluminescence

Hua Lai[b], Ying Du[a,b], Min Zhao[b], Kening Sun[a,b], Lei Yang[b,*]

[a]State Key Laboratory of Urban Water Resource and Environment, School of Municipal and Environmental Engineering, Harbin Institute of Technology, Harbin, Heilongjiang 150090, PR China

[b]Natural Science Research Center, Academy of Fundamental and Interdisciplinary Sciences, Harbin Institute of Technology, Harbin, Heilongjiang 150080, PR China

Received 3 June 2013; received in revised form 12 July 2013; accepted 19 July 2013
Available online 26 July 2013

Abstract

In this paper, we report a simple and convenient method toward fabrication of $YPO_4:Eu^{3+}$ with controlled crystal structures, morphologies and enhanced luminescent intensity. By simply adding different organic additives during the hydrothermal process, tetragonal $YPO_4:Eu^{3+}$ and hexagonal $YPO_4 \cdot 0.8H_2O:Eu^{3+}$ with nano-/microstructures can be obtained. Meanwhile, the possible formation mechanisms for products with different structures and morphologies have been presented. Furthermore, the luminescent properties of YPO_4:Eu with different structures and morphologies were also studied and compared. We believe the method reported here could open a novel approach to rare earth phosphates with multiple structures.

Keywords: $YPO_4:Eu^{3+}$; Organic additives; Controlled; Luminescent properties

1. Introduction

Lanthanide compounds have been widely used as high-performance luminescent devices, magnets, catalysts, time-resolved fluorescence labels for biological detection, and other functional materials based on the optoelectronic and chemical characteristics resulting from the 4f shell of their ions [1–6]. In modern chemistry and materials science, phase control of nanocrystals is quite important in preparative chemistry and materials science, because inherent nanocrystal structures of materials play crucial roles in both physical and chemical properties.

It is well known that the properties of a material depend on nanostructures that can be tuned through the preparation methods. So far, $YPO_4:Eu^{3+}$ has been prepared by various methods, such as sol–gel [7], hydrothermal [8], coprecipitation method [9], and so on [10–12]. Among them, hydrothermal synthetic route allows to synthesize highly crystallized powders with a narrow particle size distribution and high purity without further heat treatment at high temperatures. Several research teams have used the hydrothermal method to synthesize YPO_4, and found that the required phase could not be obtained by changing the temperature and pH of the solution, while can be obtained by adding organic additive. For example, Lin et al. synthesized metastable zircon-type YPO_4:Eu nanocrystals at a low temperature using the trisodium citrate (Cit^{3-}) assisted hydrothermal method [13]. Mai et al. reported the synthesis of $YPO_4:Eu^{3+}$ architectures with organic acids and amines as the additive [14]. However, all these methods can singly control the shape or the crystal structure, whereas reports about controlling both morphology and crystal structure simultaneously are extreme rare, and we believe such research is very important because it can not only provide new methods for the controllable preparation of rare earth orthophosphates, but also help us further understand the effect of morphology and crystal structure on the luminescent property.

In this paper, by using different organic additives in the hydrothermal process, we prepared $YPO_4:Eu^{3+}$ with controlled

*Corresponding author. Tel./fax: +86 045186412153.
E-mail address: leiyanghit@163.com (L. Yang).

0272-8842/$ - see front matter © 2013 Elsevier Ltd and Techna Group S.r.l. All rights reserved.
http://dx.doi.org/10.1016/j.ceramint.2013.07.094

structures, morphologies, and luminescent property. It is found that organic additives, such as citric acid, oxalate and ethylene diamine tetraacetic acid (EDTA) favor the formation of hexagonal $YPO_4 \cdot 0.8H_2O$ and can induce the formation of polymorph, such as nanospheres, nansorods, and microprisms. Then we concentrate on the luminescence properties of YPO_4:Eu (8%) with different structures and morphologies. The paper reports a simple method to realize the selective synthesis of YPO_4:Eu, which not only has great theoretical significance in studying the phase transition processes and the structure-dependent properties but also is very important for their potential applications.

2. Experimental

In a typical synthesis process, 10 mL $Y(NO_3)_3$ (0.2 M) was added into 20 mL aqueous solution containing a certain amount of organic additive (citric acid, oxalate, and EDTA) to form the Y^{3+} – organic additive – complex. And then the pH of the solution was rapidly adjusted to 8 by addition of $NH_3 \cdot H_2O$ solution. Afterwards, $NH_4H_2PO_4$ (0.5 M, 6 mL) solution was added slowly to the above solutions. After additional vigorous stirring for about 30 min, the solution was transferred into a stainless steel autoclave with an inner Teflon vessel (volume, 50 mL). The autoclave was sealed, maintained at a certain temperature for different times and was naturally cooled to room temperature. After the reaction was complete, the resulting solid product was centrifuged, washed with deionized water and alcohol to remove ions possibly remaining in the final products, and finally dried at 80 °C in air for further characterization. In this way, the hexagonal YPO_4 was synthesized by the solution with different Y/organic additive molar ratio. YPO_4:Eu (8%) samples were prepared by a similar procedure.

The powder X-ray diffraction (XRD) patterns were recorded on a Rigaku D/max-2000 diffractometer with Cu Kα radiation ($\lambda = 1.5418$ Å). Infrared spectra of powders (FTIR) were recorded in the range of 500–4000 cm^{-1} on a Fourier transform spectrometer. Scanning electron micrographs (SEM) were taken on a JSM-6700F field-emission scanning electron microscope (FE-SEM). Photoluminescence (PL) spectra were recorded on a RF-5301PC with Xe lamp at room temperature.

3. Results and discussion

3.1. Structural analysis

Fig. 1 shows the XRD patterns of the as-synthesized YPO_4:Eu samples under hydrothermal treatment at 180 °C for 12 h without additives (a) and with different additives: Cit^{3+} (b), oxalate (c), and EDTA (d). It can be seen that all the samples are well crystalline, and the sample prepared without additives shows diffraction peaks that can be well indexed to dehydrated YPO_4 with tetragonal xenotime structure (JCPDS File no. 84-0335). When the additive is used, the structure of the sample is changed and the hexagonal $YPO_4 \cdot 0.8H_2O$ (JCPDS No. 42-0082) can be observed. Noticeably, no peaks of any other impurities are detected, which demonstrates that pure phase products can be obtained by this synthesis method, and the additive has a significant effect on the crystal phases of the products.

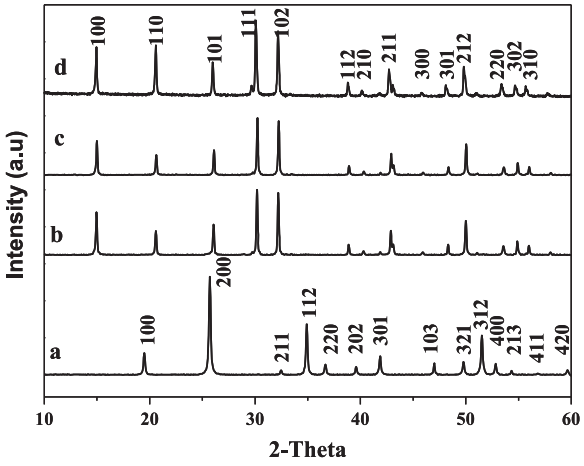

Fig. 1. XRD patterns of the as-synthesized YPO_4 samples under hydrothermal treatment at 180 °C for 12 h without additives (a) and with different additives: citric acid (b), oxalate (c), and EDTA (d).

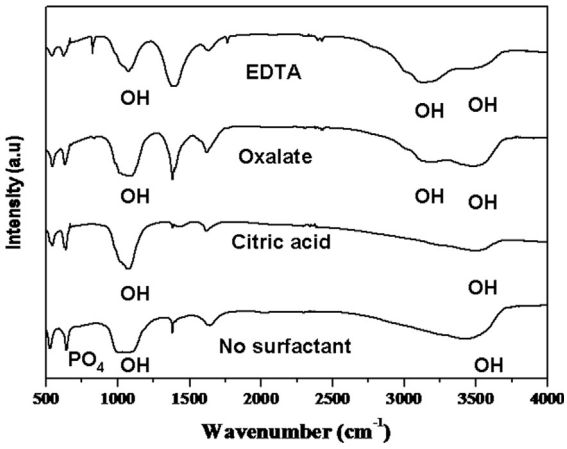

Fig. 2. IR spectra of the as-synthesized YPO_4 samples under hydrothermal treatment at 180 °C for 12 h without additives and with different additives as labeled.

The purity of the products was further examined through the FT-IR measurements. The IR spectra of as-prepared YPO_4:Eu prepared under hydrothermal treatment 180 °C for 12 h without additive and with additives (citric acid, oxalate, and EDTA) are shown in Fig. 2. The peaks appearing at 531–620 cm^{-1} and 957–1063 cm^{-1} correspond to the bending vibrations (u4 region) and stretching vibrations (u3 region) of PO_4^{3-} group, respectively [15–17]. No other phosphorus-containing groups such as $P_2O_7^{4-}$ (typically located at 1265–1267 cm^{-1}) are observed [18,19], showing that the as-synthesized product has a high purity. The band around 1400 cm^{-1} corresponds to the vibration of residual NO_3^- groups [20] originating from the starting reactants ($LnNO_3$). An absorption at 2350 cm^{-1} can be assigned to stretching vibration of Y–O. Peaks centered at 1628 and 3482 cm^{-1} belong to the bending and stretching vibrations of O–H group, respectively.

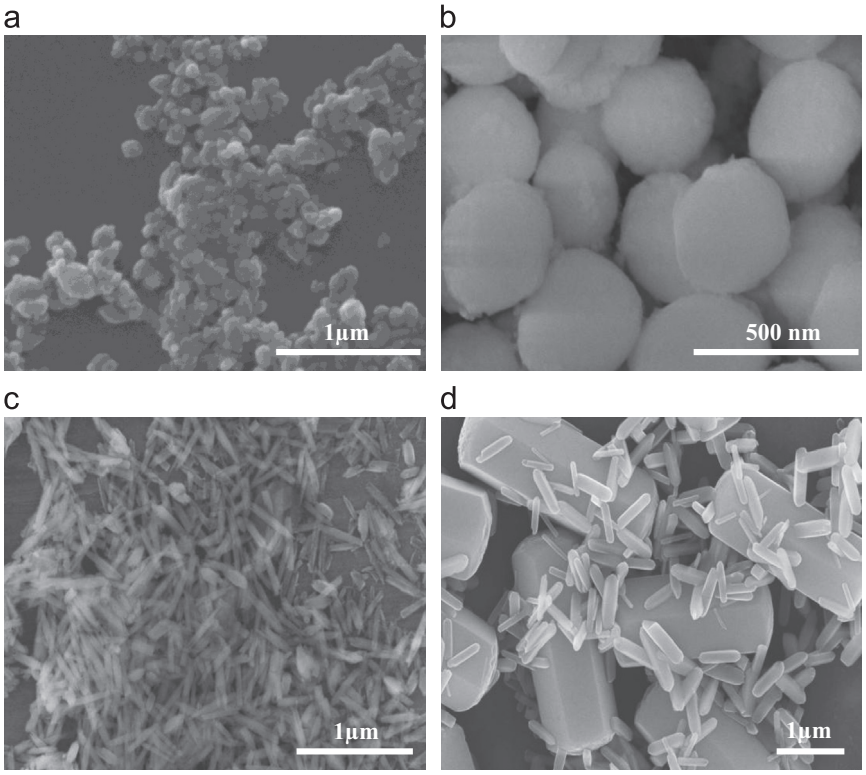

Fig. 3. SEM images of YPO_4 powders hydrothermally synthesized under hydrothermal treatment for at 180 °C for 12 h without additives (a) and with different additives: citric acid (b), oxalate (c), and EDTA (d).

3.2. Morphology analysis

The morphologies of the as-prepared samples were examined by the scanning electron microscope (SEM). As shown in Fig. 3a, the obtained samples prepared at 180 °C for 12 h without any organic additive are composed of nanoparticle, with the average diameter ranging from 40 to 100 nm. After use of organic additive (other reaction conditions are constant), the morphology of the as-prepared samples would be rather different. When the citric acid is used in the original hydrothermal environment, the sample consists of spheres with the average diameter ranging from 80 to 200 nm can be observed (Fig. 3b). Noticeably, the sizes of the samples obtained with citric acid are obviously larger than those prepared without additive. When oxalate used as organic additive, the obtained sample consists of nanorods with diameters of about 100 nm and length from 300 to 600 nm (Fig. 3c). When EDTA was used as the organic additive, the obtained samples consist of hexagonal microprisms (about 0.7–1.3 μm in diameter and 2–4 μm nm in length) and nanorods (200 nm in diameter and 1 μm in length). These results demonstrate that the additive has a crucial role in determining the morphology of the YPO_4 and different morphologies can be realized through using different additives.

3.3. Effect of organic additives

For a better understand of the effect of additives on the morphologies of the samples, a series of time and temperature dependent experiments were carried out, and we find that both the reaction time and temperature can play important roles in controlling the morphology. Note that the crystal phase of the obtained $YPO_4 \cdot 0.8H_2O$ retains the hexagonal structure at different temperatures and reaction times. As shown in Fig. 4, for the samples prepared with citric acid, with increasing the reaction time and temperature, the intensity of the diffraction peak is increased, indicating that higher temperature and long reaction would be suitable for the fabrication of samples with good crystal structures (the variation trend of samples prepared with oxalate and EDTA is similar). Although reaction

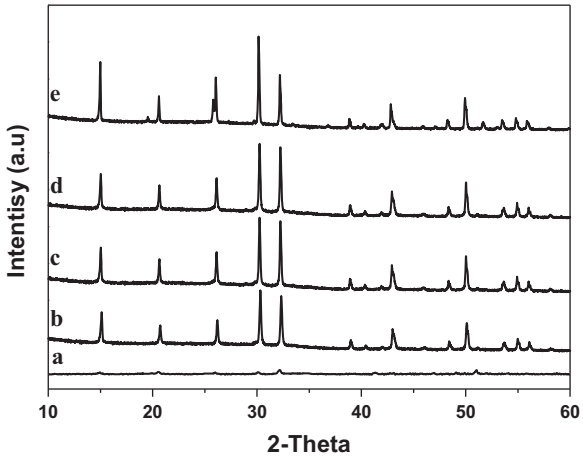

Fig. 4. XRD patterns of YPO_4 powders hydrothermally synthesized under hydrothermal treatment for at 180 °C with citric acid for different reaction times (a) 2, (b) 6, (c) and 12 h; (d, e) XRD of samples prepared with citric acid for 12 h at 120 °C and 180 °C, respectively.

temperature and time have no effect on the crystal structures, the effect on the sample morphology is remarkable. Fig. 5a–c shows the SEM images of the products obtained at 180 °C with citric acid as additive at different reaction times. When the reaction time is about 2 h, small particles were formed with an average diameter of about 50 nm (Fig. 5a). As the reaction time was prolonged to about 6 h, nanospheres with diameters ranging from 50–100 nm can be observed, and the surfaces of the spheres are coarse (Fig. 5b). Further increasing the reaction time to about 12 h, the sizes of the spheres has increased, and the surfaces become more smooth (Fig. 5c), indicating that the samples with better crystalline can be obtained through increasing the reaction time, which is in agreement with the XRD results (Fig. 4a–c). Different froms the citric acid, when the oxalate was used as the additive, the morphologies of the samples can change from the nanoparticles to the nanorods as the reaction time was increased. From Fig. 5d, it can be seen that nanoparticles with size of about 20 nm can be formed at short reaction time ($t=2$ h). Increasing the reaction time to about 6 h, nanorods with 50 nm in diameter and 100 nm in length can be observed (Fig. 5e). Further increasing the reaction time to about 12 h, both the diameter and the length of the nanorods can be increased (100 nm in diameter and 300–600 nm in length) (Fig. 5f). Fig. 5g–i shows the SEM images of the samples prepared with EDTA as the additive. At $t=2$ h, spherical-like nanoparticles (Fig. 5g) with a mean diameter of about 20–50 nm can be obtained. With the reaction proceeding to 6 h, the regular and well-defined microprisms appear with an average diameter of 0.7–1.3 μm and a length of 2–4 μm. Simultaneously, these microprisms are surrounded by a lot of nanotablets (Fig. 5h). After 12 h of growth, the morphology and size of the microprism have no apparent variation, while the nanotablets gradually grown to nanorods (200 nm in diameter and 1 μm in length), as shown in Fig. 5i. From the above, it can be concluded that the reaction time has a crucial role in determining the morphology. In addition to the reaction time, the effect of reaction temperature on the sample morphology was also investigated, and the trend of the variation is similar with the reaction time.

On the basis of the above SEM observation, a possible growth process is proposed, a simple and possible mechanism for the formation of YPO_4:Eu samples with different structures and

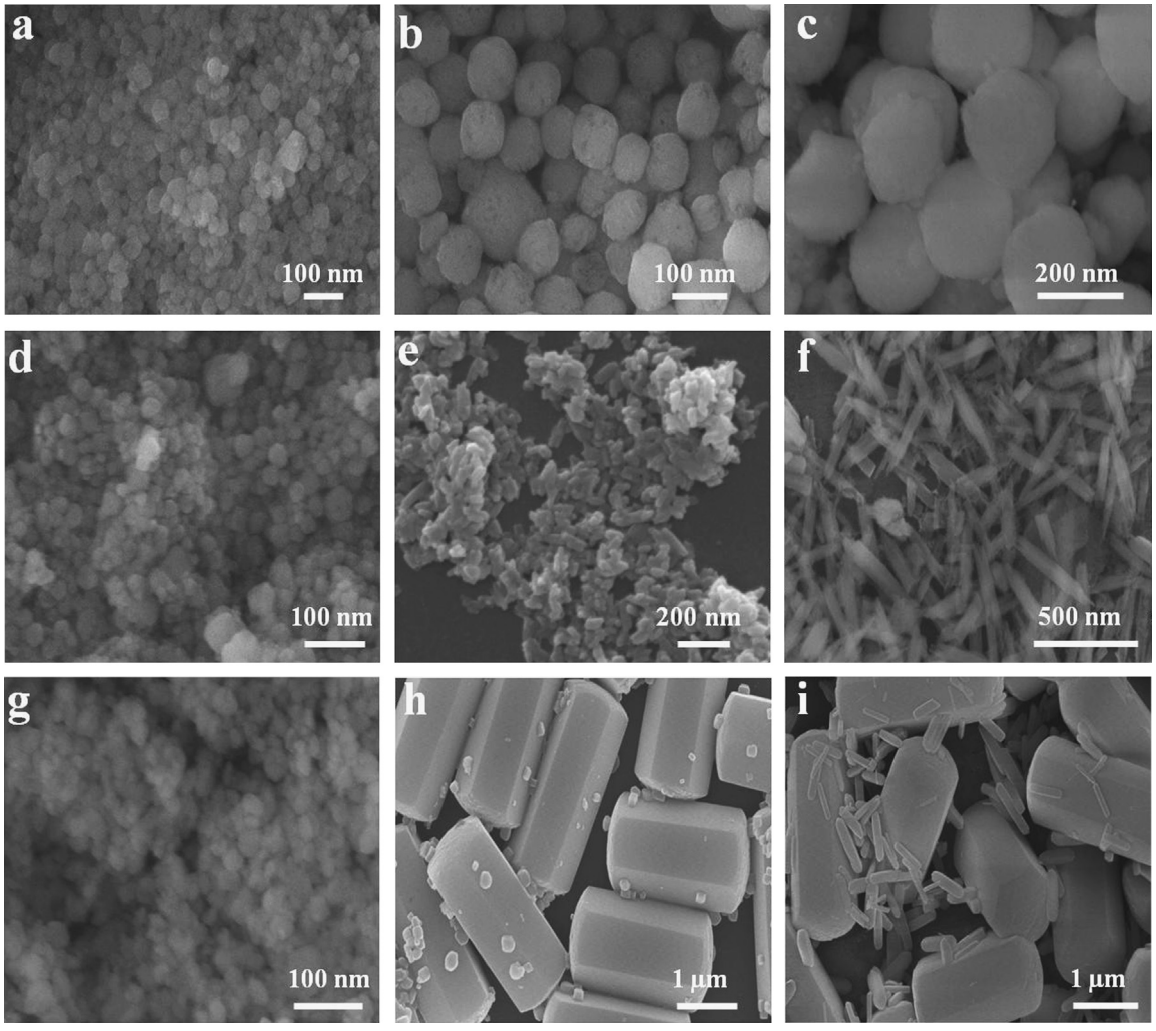

Fig. 5. SEM images of YPO_4 synthesized under hydrothermal treatment at 180 °C with different additives for different reaction time: (a, b, c) citric acid for 2 h, 6 h, and 12 h, respectively; (d, e, f) oxalate for 2 h, 6 h, and 12 h, respectively; and (h, i, j) EDTA for 2 h, 6 h, 12 h, respectively.

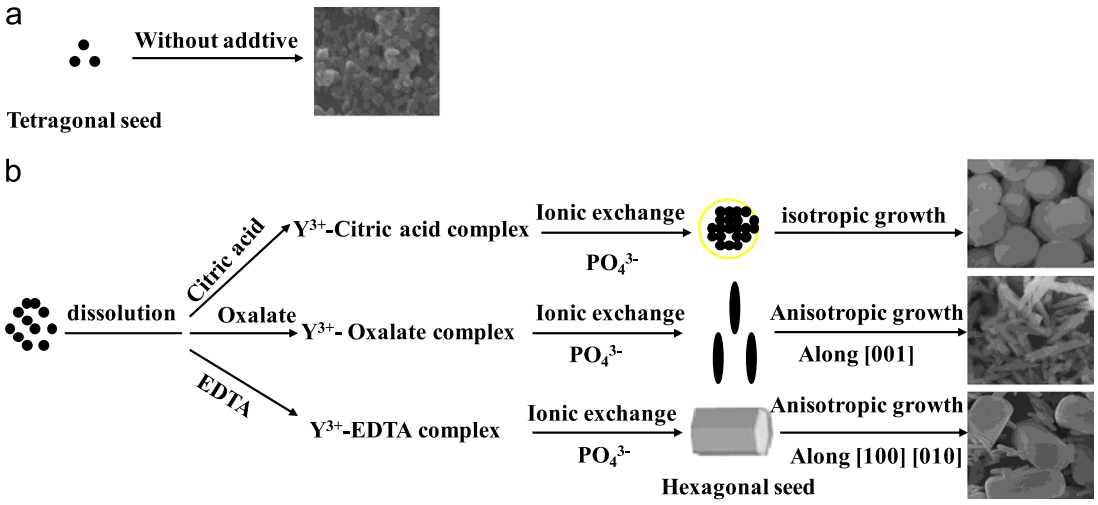

Fig. 6. Possible formation mechanisms of YPO_4 samples with different morphologies under hydrothermal condition prepared in the presence of additives.

morphologies under hydrothermal process are schematically presented in Fig. 6. Without the usage of additive, tetragonal phase would be favorable for YPO_4 nanoparticles due to its intrinsic structure and isotropy nature [21] (Fig. 6a). When the additives were used, the organic ligand can form Y^{3+}-additives (Y^{3+}–citric acid, Y^{3+}–oxalate and Y^{3+}–EDTA) complexes through stronger coordination interaction. According to LaMer's model, the formation of such complexes could control the concentration of free Y^{3+} ion concentration in solution, and thus help to control the nucleation and growth of the crystals in the view of dynamic process [22]. Then under the hydrothermal conditions the chelating of Y^{3+}-additive complexes would be weakened and an anion-exchange reaction between PO_4^{3-} and additive would take place. This competition reaction gives rise to the formation of YPO_4 nuclei. The strong steric hindrance of ligand and repulsion between coordinating atoms forced YPO_4 to crystallize in the hexagonal phase with lower symmetry [23]. In additive to the crystal structures, the additive can also affect the sample morphologies (Fig. 3). In a solution-phase synthesis, organic additives acting as surfactants or capping agents can change the order of free energies of different facets through their interaction with metal surface. This alteration may significantly affect the relative growth rates of different facets, [13] resulting in different morphologies. Meanwhile, the various architectures still undergo the Ostwald ripening process at the cost of the smaller nanoparticles, thus, as shown in Fig. 5, the size of the as-obtained various architectures increases with the reaction time. It is worth noting that because different additives have different abilities of chelating, which would result in the different growth environment of the crystals. For the Cit^{3+}, which is a kind of organic ligand with three carboxylate groups, and these carboxylate groups can form Y^{3+}–Cit^{3-} complexes through strong coordination. As we know, the Y^{3+}–Cit^{3-} complexes slows down the nucleation and subsequent crystal growth of the precursor architecture. The relatively slow generation rate of nanoparticles would be favorable for the subsequent growth of sphere nanostructures (Fig. 6b). Compared with the Cit^{3+}, the oxalate with two carboxylate groups and shorter alkyl chain, which would lead to the increased ability of chelating [14], and ultimately can strength growth of sideways along the [001] direction, resulting in the formation of the final nanorod shape. As for the EDTA, it has proved that diethylamine and NH_2-bearing ligands are very effective in guiding the growth of 1D nanostructure [24], meanwhile, EDTA has four carboxylate groups comparing to oxalate, so the Y^{3+}–EDTA complex is more stable, and thus hexagonal YPO_4 microprism (nanorod) with relatively large size can be obtained.

3.4. Photoluminescence properties

3.4.1. Different crystal phases

We first investigate the photoluminescence properties of 8 mol% Eu^{3+}-doped $YPO_4 \cdot 0.8H_2O$ with hexagonal structure and YPO_4 with tetragonal structure (both of the two sample are nanoparticles). The excitation spectra (Fig. 7a) of two samples consist of a broadband caused by the oxygen-to-europium charge transfer band (CTB) and a group of sharp lines arising from the f–f transition within the Eu^{3+} $4f^6$ electron configuration. By a comparison of the two excitation spectra, it can be clearly seen that the position of CTB for hexagonal $YPO_4 \cdot 0.8H_2O$:Eu shows obvious red-shift with respect to that for tetragonal YPO_4:Eu, as marked with red dot lines. It is well known that the CTB position depends on the Eu–O bond length: the longer the Eu–O bond length, the longer wavelength of the CTB. [14] Therefore, the nearly 7 nm red-shift indicates that the average Eu–O bond distance is somewhat longer in hexagonal $YPO_4 \cdot 0.8H_2O$:Eu than in tetragonal YPO_4:Eu. The emission spectra (Fig. 7b) are composed of $^5D_0 \rightarrow {}^7F_J$ ($J=1$, 2, 3, and 4) emission lines of Eu^{3+}, with the magnetic-dipole (MD) transition $^5D_0 \rightarrow {}^7F_1$ orange emission being the most prominent group. Furthermore, the intensity of emission spectrum of $YPO_4 \cdot 0.8H_2O$:Eu is higher than tetragonal YPO_4:Eu. We think that the reasons responsible for the difference of luminescence intensities should have two aspects. First, the distortion and covalence degree of the Eu^{3+} site are different because of their different crystal phases; the YPO_4 with a hexagonal crystal structure offers a crystal site with a C_n

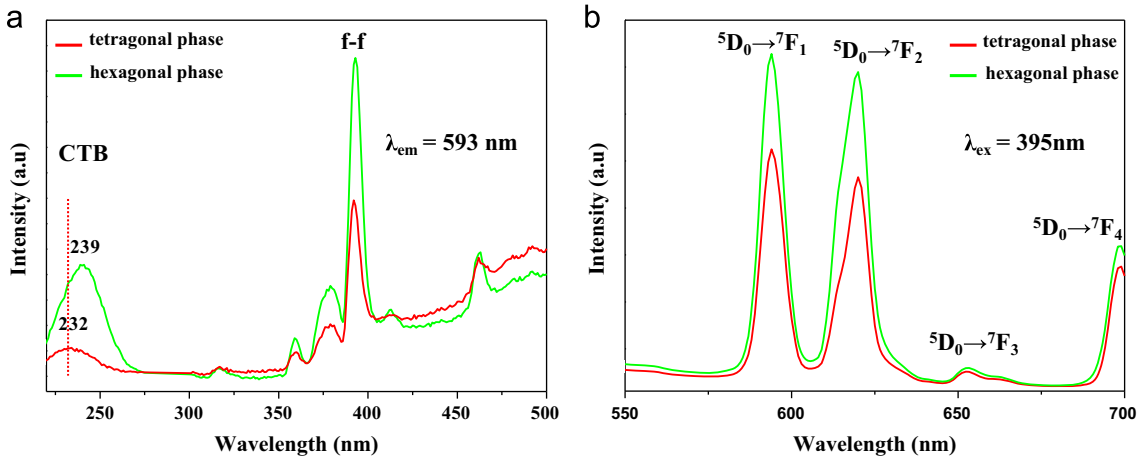

Fig. 7. Excitation (a) and emission (b) of $YPO_4 \cdot 0.8H_2O$:Eu (8%) with different crystal structures hydrothermally synthesized at 180 °C for 12 h.

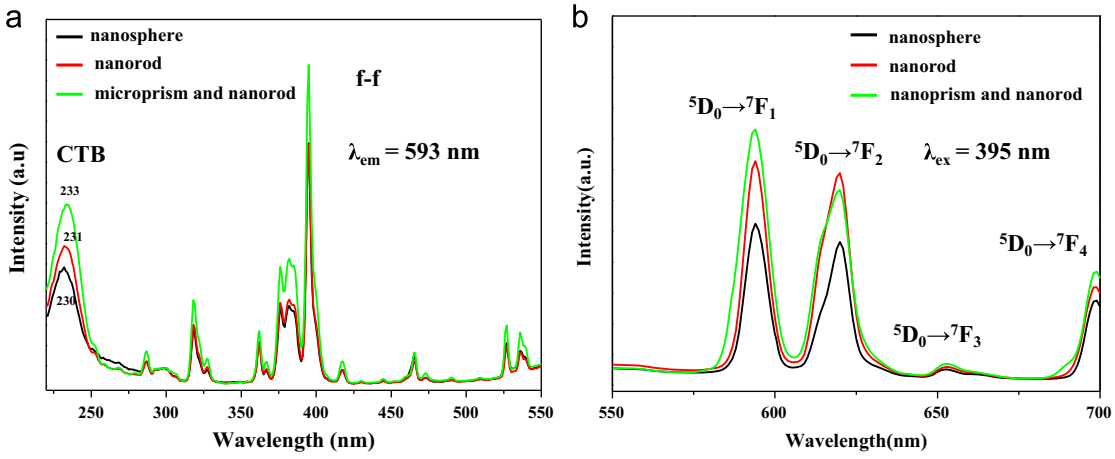

Fig. 8. Excitation (a) and emission (b) of hexagonal $YPO_4 \cdot 0.8H_2O$:Eu (8%) samples hydrothermally synthesized at 180 °C for 12 h with different shapes.

space group which has very low inversion symmetry [24] and can results in a higher intensity of the transitions. Second is the difference in their sizes. The sample of tetragonal YPO_4:Eu shows nanoparticles shape with the diameter ranging from 40 to 100 nm, whereas the sample of hexagonal $YPO_4 \cdot 0.8H_2O$:Eu has spheres shape with the diameter is 80–200 nm. The increase in samples size may causes the perfection of order of atomic arrangement and leads to higher oscillating strengths for the optical transitions.

3.4.2. *$YPO_4 \cdot 0.8H_2O$:Eu with different shapes*

Fig. 8a and b shows the representative excitation and emission spectrum of $YPO_4 \cdot 0.8H_2O$:Eu samples hydrothermal synthesized at 180 °C for 12 h with different shapes: hexagonal sphere (citric acid), hexagonal nanorod (oxalat), and hexagonal sbmicrorism and nanorod (EDTA). The excitation spectra of three samples consist of a broadband caused by the oxygen-to-europium charge transfer band (CTB) and a group of sharp lines arising from the f–f transition within the Eu^{3+} $4f^6$ electron configuration. Moreover, the position of CTB slightly changes for the three samples due to different Eu–O bond length. The emission spectra of the $YPO_4 \cdot 0.8H_2O$:Eu with different shapes composed of sharp lines ranging from 500 to 700 nm are associated with the transitions from the excited $^5D_0$ level to the ^7F_J ($J=1$, 2, 3, and 4) levels of Eu^{3+} activators (Fig. 8b). The emission bands around 593 nm can be ascribed to the $^5D_0 \rightarrow {}^7F_1$ magnetic dipole transitions. Meanwhile, the emission peaks located at about 615 nm are mainly due to the transitions from $^5D_0$ to $^7F_2$ energy levels. The $^5D_0 \rightarrow {}^7F_2$ transition is a forced electronic dipole–edipole transition. Noticeably, a remarkable difference in the spectral intensity is observed. The sample prepared with citric acid has the lowest intensity, and then the sample prepared with oxalat, the intensity of sample prepared with EDTA is the highest. Although different additives are used, the crystal phase of the three products is the same, i.e., hexagonal $YPO_4 \cdot 0.8H_2O$. So it is reasonable to believe that the different luminescence properties of the products arise from their morphologies and sizes. The luminescence intensity of the hexagonal nanorod prepared with oxalat is higher than nanosphere prepared with citric acid can be attributed to the variation of dipole field caused by the shape anisotropy, which can affect the ionic dipole field, the photonic density states and the radiative transition rate. When the EDTA is used, larger size microprisms and nanorods can be obtained compared with those prepared with oxalat. Small

nanorods possess more grain boundaries compared to large miroprism and nanorod. In these grain boundaries, dangling bonds or disorder of atomic arrangement takes place, which act as primary quenching centers in luminescence because of multi-phonon relaxation. Therefore, an increase in samples size causes the perfection of order of atomic arrangement and leads to higher oscillating strengths for the optical transitions [25], thus, the samples prepared with EDTA has a higher intensity than those prepared with oxalat.

4. Conclusion

In summary, YPO_4 powders with different crystal structures and morphologies were hydrothermally synthesized at 180 °C for 12 h with the assistance of different organic additives, namely: citric acid, oxalate, and EDTA. It is found that organic additives can induce the polymorph transformation from tetragonal YPO_4 to hexagonal $YPO_4 \cdot 0.8H_2O$, meanwhile, different morphologies such as nanospheres, nanorods, and microprisms can also be obtained with different additives. Results of luminescent properties indicate that the luminescent intensity cannot only be controlled by the crystal phases, but also the morphology of the samples, and the samples with hexagonal structures and large size can obtain higher luminescent intensity. These findings indicate that the luminescence properties of a material are strongly related to its crystal structure, the shape, and size.

Acknoweledgment

This work is supported by the Open Project of State Key Laboratory of Urban Water Resource and Environment, Harbin Institute of Technology (No. ES201008); Project (HIT.NSRIF. 2009087 and 2009081) supported by Natural Scientific Research Innovation Foundation in Harbin Institute of Technology; the Fundamental Research Funds for the Central Universities (Grant no. HIT. NSRIF. 2010059); China Postdoctoral Science Foundation funded project (20110490105 and 2011M500650); and Innovation Talent Research Fund of Harbin Science and Technology Bureau (2009RFXX047).

References

[1] W.P. Huang, X.H. Tang, Y.Q. Wang, Y. Koltypin, A. Gedanken, Selective synthesis of anatase and rutile *via* ultrasound irradiation, Chemical Communications 15 (2000) 1415–1416.

[2] J. Lu, P.F. Oi, Y.Y. Peng, Z.Y. Meng, Z.P. Yang, W.C. Yu, Y.T. Qian, Solvothermal reactions: an original route for the synthesis of novel materials, Chemistry of Materials 13 (2001) 2169–2172.

[3] X. Wang, Y.D. Li, Selected-control hydrothermal synthesis of α- and β-MnO_2 single crystal nanowires, Journal of the American Chemical Society 124 (2002) 2880–2881.

[4] X. Wang, Y.D. Li, Synthesis and formation mechanism of manganese dioxide nanowires/nanorods, Chemistry: A European Journal 9 (2003) 300–306.

[5] X.J. Chen, H.F. Xu, N.S. Xu, F.H. Zhao, W.J. Lin, G. Lin, Y.L. Fu, Z. L. Huang, H.Z. Wang, M.M. Wu, Kinetically controlled synthesis of wurtzite ZnS nanorods through mild thermolysis of a covalent organic – inorganic network, Inorganic Chemistry 42 (2003) 3100–3106.

[6] N. Blagden, R.J. Davey, Polymorph selection: challenges for the future?, Crystal Growth and Design 3 (2003) 873–885

[7] W.H. Di, X.J. Wang, B.J. Chen, X.X. Zhao, A new sol–gel route to synthesize YPO_4:Tb as a green-emitting phosphor for the plasma display panels, Chemistry Letters 34 (2005) 566–567.

[8] Z.Y. Huo, C. Chen, D. Chu, H.H. Li, Y.D. Li, Systematic synthesis of lanthanide phosphate nanocrystals, Chemistry: A European Journal 13 (2007) 7708–7714.

[9] H. Lai, A. Bao, Y.M. Yang, Y.C. Tao, H. Yang, Y. Zhang, et al., UV luminescence property of YPO_4:RE (RE) Ce^{3+}, Tb^{3+}, Journal of Physical Chemistry C, 112 (2008) 282–286.

[10] W.H. Di, X.J. Wang, B. Chen, S.Z. Lu, X.X. Zhao, Effect of OH – on the luminescent efficiency and lifetime of Tb^{3+}-doped yttrium orthophosphate synthesized by solution precipitation, Journal of Physical Chemistry B 109 (2005) 13154–13158.

[11] Z.Y. Huo, C. Chen, Y.D. Li, Self-assembly of uniform hexagonal yttrium phosphate nanocrystals, Chemical Communications 33 (2006) 3522–3524.

[12] J.M. Nedelec, D. Avignant, R. Mahiou, Soft chemistry routes to YPO_4-based phosphors: dependence of textural and optical properties on synthesis pathways, Chemistry of Materials 14 (2002) 651–655.

[13] C.X. Li, Z.Y. Hou, C.M. Zhang, P.P. Yang, G.G. Li, Z.H. Xu, Y. Fan, J. Lin, Controlled synthesis of Ln^{3+} (Ln=Tb, Eu, and Dy) and V^{5+} ion-doped YPO_4 nano-/microstructures with tunable luminescent colors, Chemistry of Materials 21 (2009) 4598–4607.

[14] H.X. Mai, Y.W. Zhang, L.D. Sun, C.H. Yan, Orderly aligned and highly luminescent monodisperse rare-earth orthophosphate nanocrystals synthesized by a limited anion-exchange reaction, Chemistry of Materials 19 (2007) 4514–4522.

[15] M. Ferhi, K. Horchani-Naifer, M. Ferid, Combustion synthesis and luminescence properties of $LaPO_4$:Eu (5%), Journal of Rare Earths 27 (2009) 182–186.

[16] G.M. Begun, G.W. Beall, L.A. Boatner, W.J. Gregor, Raman spectra of the rare earth orthophosphates, Journal of Raman Spectroscopy 11 (1981) 273–278.

[17] K. Nakamoto, Infrared and Raman Spectra of Inorganic and Coordination Compounds, Wiley, New York, 1986.

[18] C.R. Patra, G. Alexandra, S. Patra, D.S. Jacob, A. Gedanken, A. Landau, Y. Gofer, Microwave approach for the synthesis of rhabdophane-type lanthanide orthophosphate (Ln=La, Ce, Nd, Sm, Eu, Gd and Tb) nanorods under solvothermal conditions, New Journal of Chemistry 29 (2005) 733–739.

[19] S. Lucas, E. Champion, D. Bernache-Assollant, G. Leroy, Rare earth phosphate powders $RePO_4 \cdot nH_2O$(Re=La,Ce or Y) – Part II. Thermal behavior, Journal of Solid State Chemistry 177 (2004) 1312–1320.

[20] G.H. Pan, H.W. Song, X. Bai, Z.X. Liu, H.Q. Yu, W.H. Di, S.W. Li, L. B. Fan, X.G. Ren, S.Z. Lu, Novel energy-transfer route and enhanced luminescent properties in YVO_4:Eu^{3+}/YBO_3:Eu^{3+} composite, Chemistry of Materials 18 (2006) 4526–4529.

[21] Y.P. Fang, A.W. Xu, R.Q. Song, H.X. Zhang, L.P. You, J.C. Yu, H. Q. Liu, Systematic synthesis and characterization of single-crystal lanthanide orthophosphate nanowires, Journal of the American Chemical Society 125 (2003) 16025–16034.

[22] Z.Q. Li, Y. Zhang, Monodisperse silica-coated polyvinylpyrrolidone/$NaYF_4$ nanocrystals with multicolor upconversion fluorescence emission, Angewandte Chemie International Edition 45 (2006) 7732–7735.

[23] C.H. Jia, L.D Sun, L.P. You, X.C. Jiang, F. Luo, Y.C. Pang, C.H. Yan, Selective synthesis of monazite- and zircon-type $LaVO_4$ nanocrystals, Journal of Physical Chemistry B 109 (2005) 3284–3290.

[24] R.X. Yan, X.M. Sun, X. Wang, Q. Peng, Y.D. Li, Crystal structures, anisotropic growth, and optical properties: controlled synthesis of lanthanide orthophosphate one-dimensional nanomaterials, Chemistry: A European Journal 11 (2005) 2183–2195.

[25] L.X. Yu, H.W. Song, S.Z. Lu, Z.X. Liu, L.M. Yang, X.G. Kong, Luminescent properties of $LaPO_4$:Eu nanoparticles and nanowires, Journal of Physical Chemistry B 108 (2004) 16697–16702.